Structural determination of indium-induced Si(111) reconstructed surfaces by LEED analysis: $(\sqrt{3}\times\sqrt{3})R30°$ and (4×1)

S. Mizuno,[1,2] Y. O. Mizuno,[1] and H. Tochihara[1]
[1]*Department of Molecular and Material Sciences, Kyushu University, Kasuga, Fukuoka 816-8580, Japan*
[2]*PRESTO, Japan Science and Technology Corporation, Kawaguchi, Saitama 332-0012 Japan*
(Received 16 February 2003; published 20 May 2003)

Two indium-induced Si(111) reconstructed surfaces, the $(\sqrt{3}\times\sqrt{3})R30°$ and the (4×1) structures, were examined by dynamical low-energy electron diffraction I-V analysis. As suggested in former studies, the T_4 model of the $(\sqrt{3}\times\sqrt{3})R30°$ structure showed the best agreement with the experiments. For the (4×1) structure, we examined 45 models and selected the model proposed by a surface x-ray diffraction study as the most appropriate structure. The low-temperature phase, whose diffraction pattern is (8×1)-$p1g1$ with half-order streaks, has I-V curves almost identical to those of the (4×1) phase. Therefore, the structural changes accompanying a phase transition between the (4×1) and (8×1)-$p1g1$ structures should be very small.

DOI: 10.1103/PhysRevB.67.195410 PACS number(s): 61.14.Hg

I. INTRODUCTION

It is well known that metals on the Si(111)-(7×7) surface form various periodic structures upon annealing.[1] In the case of indium, the surface periodic structure changes with increasing indium coverage, to $(\sqrt{3}\times\sqrt{3})R30°$, $(\sqrt{31}\times\sqrt{31})R9°$, (4×1), and $(\sqrt{7}\times\sqrt{3})$. The Si(111)-$(\sqrt{3}\times\sqrt{3})R30°$-In [hereafter, the $(\sqrt{3}\times\sqrt{3})$] is formed at an indium coverage of 1/3 of the monolayer (ML), and the Si(111)-(4×1)-In [the (4×1)] is formed at 0.5–1 ML. The $(\sqrt{3}\times\sqrt{3})$ has been extensively studied using various techniques, including low-energy electron diffraction[2] (LEED), scanning tunneling microscopy[3] (STM), low-energy ion scattering spectroscopy[4] (ISS), medium-energy electron diffraction[5] (MEED), and impact collision ion scattering spectroscopy[6] (ICISS). These studies and total-energy calculations[7,8] have revealed that indium atoms locate at the T_4 site. The atomic positions have been also determined by both surface x-ray diffraction[9] (SXRD) and reflection high-energy electron diffraction[10] (RHEED) analysis.

Some fascinating properties of the (4×1) structure have been revealed in numerous experimental studies. STM studies indicated that the (4×1) structure consists of indium chains along the $\langle110\rangle$ direction.[11,12] In angle-resolved photoelectron spectroscopy[13] (ARPES) and inverse PES studies,[14,15] the electronic structure on the (4×1) at room temperature (RT) showed metallicity only along the chains and semiconductivity perpendicular to the chains ($\langle112\rangle$ direction). Recent ARPES studies demonstrated that the one-dimensional metallic nature of the chain changes to be semiconductive below 100 K.[16,17] In addition, charge density modulation along the chains was observed by STM on cooling at 65 K. This modulation might indicate the Peierls transition.[16]

To clarify the characteristics of the phase transition, it is first essential to ascertain the atomic arrangement. Various (4×1) structural models have been proposed using various experimental techniques: ICISS, Auger electron diffraction (AED), STM, transmission electron microscopy (TED), and SXRD.[18–24] Remarkably, the latest SXRD analysis[24] might have determined the atomic positions of the (4×1) structure. Besides the experimental studies, several theoretical studies have been done very recently.[25–27] The results of the calculations are in good agreement with those obtained from the previous SXRD study.[24] However, the problem regarding the coverage of indium remains, given that another STM study[28] proposed that the coverage of indium is different from that in the SXRD model. LEED analysis, a powerful and well-established method by which atomic positions on surfaces can be determined quantitatively, had not been used in the (4×1) case prior to this study. In this study, we analyze the $(\sqrt{3}\times\sqrt{3})$ and the (4×1) reconstructed surfaces by a tensor LEED calculation and compare our results to those of previous investigations.

II. EXPERIMENT AND CALCULATION

Experiments were carried out in an ultrahigh-vacuum (UHV) chamber with a base pressure of 1×10^{-11} Torr. A boron-doped (7–17 Ω cm) Si(111) sample was cleaned by resistive heating to 1150 °C for 5 s to produce a (7×7) surface. Indium atoms were deposited on the (7×7) surface at RT by evaporating indium drops from a tantalum-foil tube until a broad (1×1) LEED pattern was observed. Indium deposition time was ca. 5 min for the $(\sqrt{3}\times\sqrt{3})$ surface and ca. 10 min for the (4×1) surface. After the deposition, the surface was annealed at 500–550 °C for 5 min to obtain a clear $(\sqrt{3}\times\sqrt{3})$ LEED pattern and at 450–500 °C for 5 min to obtain a clear (4×1) LEED pattern. On cooling the (4×1) sample, eighth-order spots and half-order streaks appeared on the (4×1) LEED pattern below 130 K. At 80 K, a clear $(8\times$"2") LEED pattern could be observed. The "2" indicates the presence of the streaks. Intensity-voltage (I-V) curves were measured in a range of 40–280 eV on a 1-eV grid at 80 K.

To determine the atomic positions, full dynamical calculations were performed using a Barbieri–Van Hove symmetrized automated tensor LEED (SAT-LEED) package.[29] Eight phase shifts were used to represent atomic scattering ($l_{max}=7$), and further structural refinement utilized 11 phase

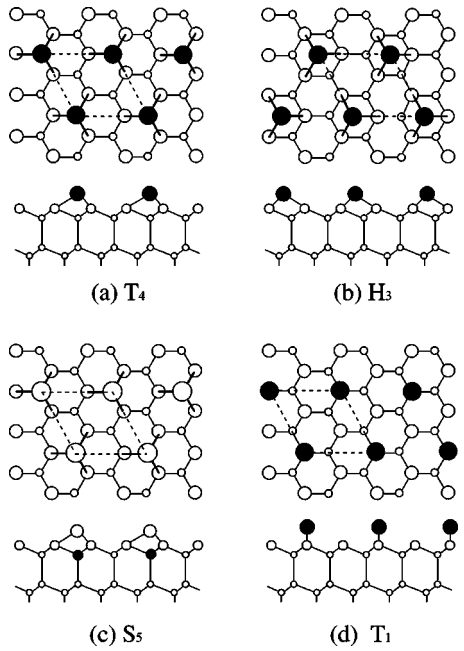

FIG. 1. Top and side views of four models examined for the Si(111)-($\sqrt{3}\times\sqrt{3}$)$R30°$-In structure. Solid and open spheres are indium atoms and silicon atoms, respectively.

shifts ($l_{max}=10$). The real part of the inner potential was determined during the theoretical- and experimental-curve fitting. The damping was represented by an imaginary part of the potential of -5.0 eV. Debye temperatures of 108 K and 640 K were used for indium and silicon atoms, respectively. The Pendry R factor (R_p) was used to direct the automated search algorithm, and the best agreement of experimental and theoretical I-V curves involved minimizing R_p.

III. RESULTS AND DISCUSSION

A. ($\sqrt{3}\times\sqrt{3}$)$R30°$ structure

Four highly symmetrical adsorption sites of indium atoms with the space group of $p31m$, shown in Fig. 1, were considered. Indium atoms on the T_4 or H_3 site saturate three silicon dangling bonds. The S_5 site is given to boron adsorption.[30] Nine symmetrically inequivalent beams were measured and used in the analysis. We allowed displacements of indium atoms and the first and second bilayer silicon atoms. The T_4 model with $p31m$ symmetry produced an R_p value of 0.135. The other three models, H_3, S_5, and on-top, had higher R_p's over 0.35 and could be ruled out. Since a double-domain ($\sqrt{3}\times\sqrt{3}$)$R30°$ structure with $p3$ symmetry can give the same LEED pattern as a structure with $p31m$ symmetry, and since the Si(111)-($\sqrt{3}\times\sqrt{3}$)$R30°$-Ag surface has a symmetry-broken structure with $p3$ symmetry below 62 K,[31] the T_4 model was recalculated using $p3$ symmetry. However, in several loops of calculation, the atomic positions did not converge into definite values. That is, the symmetry-broken T_4 model at low temperature (LT) could be ruled out at this stage. For the final structural refinement of the T_4 model, indium and three silicon bilayers were displaced using $l_{max}=10$, and the subsequent R_p value was slightly reduced to 0.127. The R-factor value of Zanazzi-Jona, R_{zj}, of this structure was 0.054, which was sufficiently small when compared with the R_{zj} values for the Si(111)-($\sqrt{3}\times\sqrt{3}$)$R30°$-B, -Al, and -Ga (group-13 elements) structures, the values of which were 0.211, 0.177, and 0.15, respectively, in previous LEED studies.[30,32,33] Experimentally measured I-V curves and theoretically calculated ones for the optimized T_4 structure fit very well, as shown in Fig. 2.

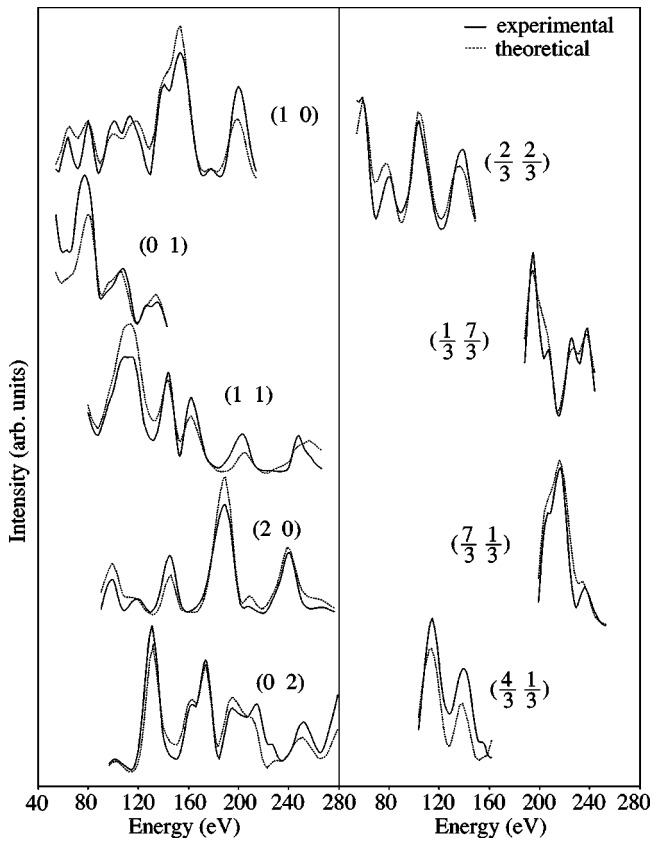

FIG. 2. Comparison between the experimental and the best-fit theoretical I-V curves for the Si(111)-($\sqrt{3}\times\sqrt{3}$)$R30°$-In structure.

The optimized parameters are listed in Table I along with the errors obtained from the variance of the R_p, $\Delta R_p = R_{min}(8V_{0i}/E_t)^{1/2}$, where ΔR_p, R_{min}, and V_{0i} are the error of R_p, the minimum R_p, and the imaginary part of the inner potential, respectively.[34] Directions of silicon atom displacements from bulk positions are indicated by arrows in Fig. 3. Our results for two bilayers and three bilayers gave consistent parameter values and showed good convergence in the analysis. Silicon atoms in the first layer have little perpendicular displacement and a lateral displacement of 0.08 Å towards the indium adatom. Silicon atoms in the second and third layers have large perpendicular displacements. Si atoms under the indium adatom, Si2a and Si3a, relax downwards by 0.36 Å and 0.25 Å, respectively. By contrast, other Si atoms in the second layer (Si2b) and in the third layer (Si3b) relax upwards by 0.07 Å and 0.04 Å, respectively. Silicon atoms in the fourth layer have only slight perpendicular displacements. Silicon atoms below the fourth layer maintain the bulk positions within the error range.

TABLE I. Optimum parameters of the best-fit structure of Si(111)-($\sqrt{3}\times\sqrt{3}$)$R30°$-In structure illustrated in Fig. 3. The perpendicular distances and lateral displacements refer to bulk-terminated sites.

	LEED (present) Two bilayers	LEED (present) Three bilayers	RHEED (Ref. 10) Two bilayers	SXRD (Ref. 9) Two bilayers	SXRD (Ref. 9) Three bilayers
Height difference (Å)					
h(In-Si1)	1.73±0.05	1.73±0.04	1.83±0.01	1.85±0.05	1.61
Perpendicular distances (Å)					
d(Si1)	−0.01±0.02	−0.04±0.02	0.01±0.11	0.01±0.08	−0.03
d(Si2a)	−0.32±0.02	−0.36±0.04	−0.20±0.14	−0.34±0.08	−0.41
d(Si2b)	0.11±0.03	0.07±0.02	0.10±0.15	0.00±0.07	0.19
d(Si3a)	−0.22±0.06	−0.25±0.05	−0.26±0.25	−0.34±0.08	−0.34
d(Si3b)	0.08±0.03	0.04±0.03	0.11±0.15	0.00±0.08	0.16
d(Si4)	−0.02±0.03	−0.05±0.03			0.01
d(Si5)		−0.01±0.06			0.01
d(Si6)		−0.04±0.04			0.01
Lateral displacement (Å)					
u(Si1)	−0.09±0.09	−0.08±0.07	−0.02±0.13	−0.20±0.01	−0.20±0.01 [a]
u(Si4)	0.03±0.22	0.03±0.23		0.14±0.01	0.12±0.01
u(Si5)		−0.06±0.18			0.01
u(Si6)		−0.02±0.13			−0.01
Bond length (Å)					
In-Si1	2.74	2.75	2.86	2.74±0.03	2.58

[a]In Ref. 9, u(Si1) is 1.196 Å. According to the other values, however, it should be 0.196 Å.

The tendency of these relaxations almost agrees with the SXRD and the RHEED analysis.[9,10] The perpendicular displacements of the second and third layer atoms show particularly good agreement. Only the lateral displacements of Si1 and Si4 atoms differ between SXRD and other methods. The lateral displacement of Si1 is extremely large in SXRD; while the error bars of lateral displacements in LEED and RHEED are large. However, the directions of displacements are identical.

Because the Debye-Waller factors of indium according to SXRD were large, the accuracy of the atomic position of indium should be checked by LEED for the ($\sqrt{3}\times\sqrt{3}$) structure before analysis of the (4×1) structure. In the case of gallium, which is also a group-13 element and forms the same ($\sqrt{3}\times\sqrt{3}$) structure, extremely large anisotropic thermal vibrations have been reported.[35] The giant vibrations are prominent at higher temperatures (e.g., 830 K), but the vibrations become moderate at RT. In this study, the influence of the vibration amplitude was decreased by cooling the sample at 80 K. We fixed the Debye temperature of the indium in this study because we did not want to increase the number of parameters during determination of the most probable model among many models. The obtained structural parameters of indium atoms are comparable to those obtained by RHEED and SXRD. The bond length between indium and silicon atoms was 2.75 Å by this study. This value is almost equal to the mean bond length of the In-In and Si-Si bond lengths in the elements, 2.80 Å. These results show that the LEED analysis has the potential to determine structures of indium adsorbed silicon surfaces.

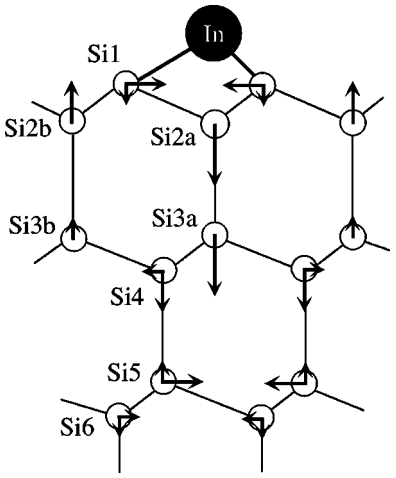

FIG. 3. Side view of the best-fit Si(111)-($\sqrt{3}\times\sqrt{3}$)$R30°$-In structure (T_4 model). Arrows indicate the directions of displacements from bulk-terminated sites.

B. (4×1) structure

A LEED pattern of the (4×1) structure at RT is shown in Fig. 4(a). When we cool down the sample at 80 K, the (4×1) structure changes to the (8×1)-$p1g1$ structure with streaks, as shown in Fig. 4(c). Schematic illustrations of the patterns with a single domain are shown in Figs. 4(b) and 4(d), respectively. Details of the (8×1)-$p1g1$ LEED pattern and the phase transition are described in the following section. At slightly higher indium coverages, we can obtain the (4×1) structure even at 80 K as reported by Ryjkov *et al.*[36] There-

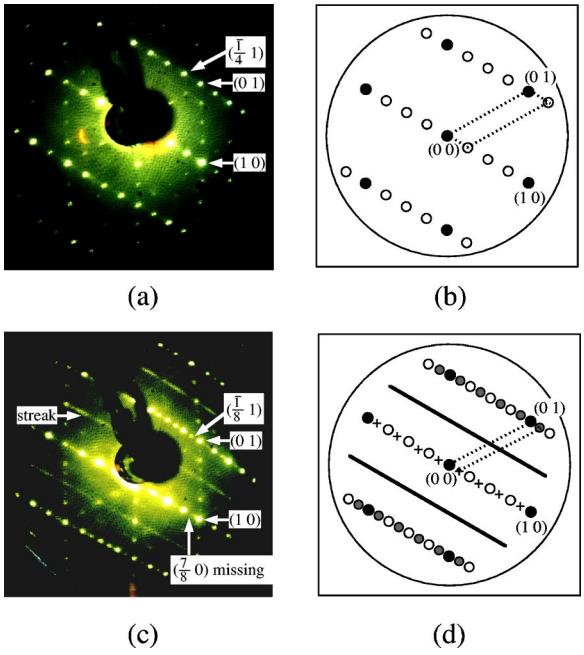

FIG. 4. (Color online) (a) A LEED pattern of the Si(111)-(4×1)-In structure at 85 eV at 300 K. (b) A schematic illustration of (a) for a single domain. (c) A LEED pattern of the Si(111)-(8×1)-$p1g1$-In with half-order streaks structure at 86 eV at 80 K. (d) A schematic illustration of (c) for a single domain.

fore, we compared the I-V curves of the (4×1) structure formed at 80 K with the I-V curves of the (4×1) structure at RT and with the I-V curves of the (8×1)-$p1g1$ structure at 80 K. Their features of both integer- and fourth-order beams are very similar, as shown in Fig. 5. It seems that the only broadening occurred at 300 K due to increase of the Debye-

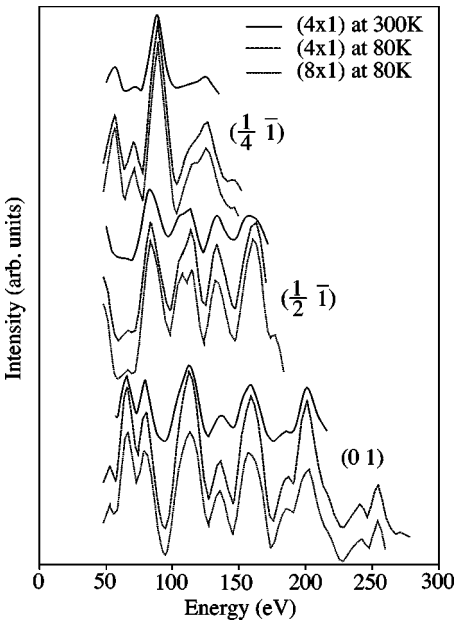

FIG. 5. Comparison between experimental I-V curves of the (4×1) structure at 300 K, of the (4×1) structure at 80 K (slightly higher indium coverage), and of the (8×1)-$p1g1$ structure at 80 K.

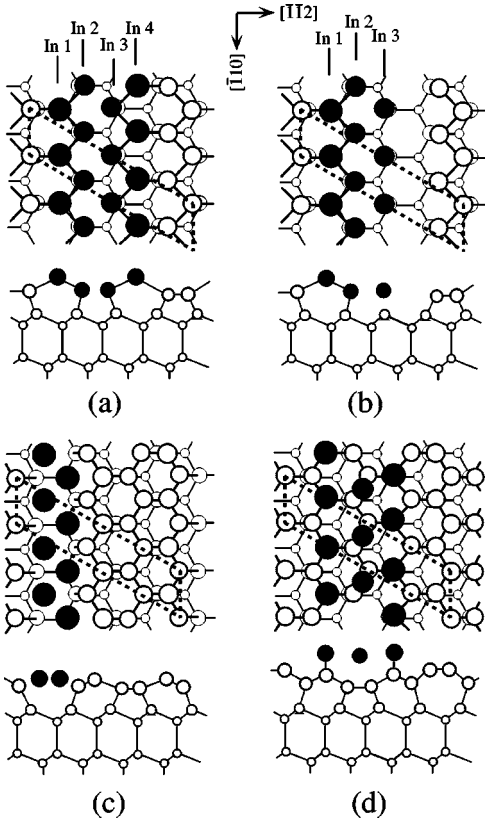

FIG. 6. Top and side views of typical models examined for the Si(111)-(4×1)-In structure. Solid and open spheres are indium atoms and silicon atoms, respectively. (a) SXRD model (model 1). (b) One of missing SXRD models (model 12). (c) TED model (model 16). (d) STM model (model 36). The dotted parallelogram indicates a (4×1) unit cell.

Waller factors. Actually, there were no significant differences in the analysis even when we used experimental I-V curves of the (8×1)-$p1g1$ structure, instead of experimental I-V curves for the (4×1) structures. Therefore, the structural changes accompanying phase transition between the (4×1) and (8×1)-$p1g1$ structures should be very small. In this study we used I-V curves of the (4×1) structure at 80 K for determination of the (4×1) structure to decrease the influence of the atomic vibration. Nine symmetrically inequivalent beams were used for the analysis. The energy range over the measured beams (E_t) was 1683 eV.

Since the core-level PES study showed that the silicon 2p spectra had two components, one from the bulk, the other from the reconstruction;[37] we specifically focused on recently proposed models with silicon reconstructions. Models from the SXRD, TED, and STM are shown in Figs. 6(a), 6(c), and 6(d), respectively. The indium coverage of these models has been shown as 1.0, 0.5, and 0.75 ML, respectively.[21–25] We made other models, modifying the coverage of each basic model by addition or removal of silicon and indium atoms. Models 2-15, models 17-35, and models 37-45 are derived from the SXRD model, TED model, and STM model, respectively. At the first step we allowed displacements of the reconstructed surface layer and one bulk bilayer. Models have 26–40 structural parameters with

TABLE II. Pendry R factor for the 45 models is examined. Coverages of indium (θ_{In}) and silicon (θ_{Si}) atoms in reconstructed layers are also shown.

Model No.	R factor	θ_{In}	θ_{Si}	Model No.	R factor	θ_{In}	θ_{Si}
1	0.257	1	0.5	24	0.499	0.75	1
2	0.382	1	0.5	25	0.363	1.25	0.5
3	0.474	1	0.5	26	0.369	1.25	1
4	0.534	1	0.5	27	0.465	0.75	1
5	0.387	0.75	0.75	28	0.425	0.75	1
6	0.423	0.75	0.75	29	0.541	0.75	1
7	0.380	0.75	0.75	30	0.459	0.75	1
8	0.486	0.75	0.75	31	0.608	1	1
9	0.537	0.5	1	32	0.477	1	1
10	0.504	0.5	1	33	0.676	1	0.75
11	0.537	0.5	1	34	0.509	0.75	0.5
12	0.278	0.75	0.5	35	0.434	0.75	0.5
13	0.292	0.75	0.5	36	0.525	0.75	2
14	0.301	0.75	0.5	37	0.384	0.75	0.5
15	0.315	0.75	0.5	38	0.443	0.75	0.5
16	0.466	0.5	1.5	39	0.420	0.75	0.5
17	0.449	0.75	1.25	40	0.375	0.75	0.5
18	0.447	0.75	1.25	41	0.428	0.75	0.5
19	0.428	0.5	1.25	42	0.453	0.75	0.5
20	0.486	0.75	1.25	43	0.462	0.75	0.5
21	0.470	0.75	1.25	44	0.424	0.75	0.5
22	0.441	0.75	0.75	45	0.587	0.75	0.5+2
23	0.483	0.75	1				

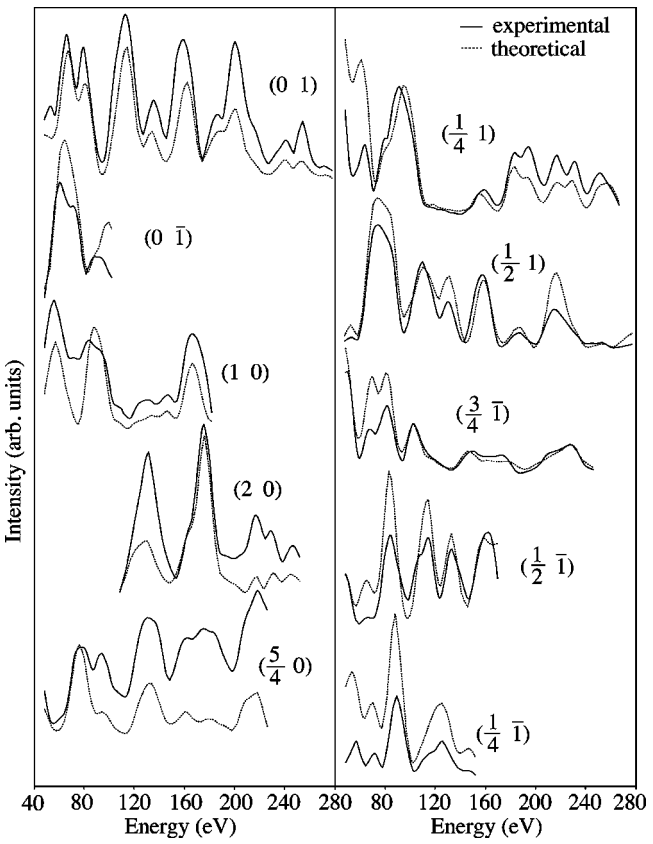

FIG. 7. Comparison between the experimental and the best-fit theoretical I-V curves for the Si(111)-(4×1)-In structure.

$p1m1$ symmetry. The list of calculated models including R_p is shown in Table II. Model 1 (SXRD model) has the lowest R_p, 0.257. The R_p of model 16 (TED model) and model 36 (STM model) are 0.466 and 0.525, respectively. Following the SXRD model, some modified SXRD models (models 12–15) have small R_p values. Since the $R_p+\Delta R_p$ of the SXRD model is 0.297, the other trial models listed in Table II can be excluded.

Model 12 has the second lowest R_p, 0.278. As shown in Fig. 6(b), model 12 has almost the same structure as the SXRD model, except that one of the four indium rows is missing. In the models 13-15, In1, In2, and In3 rows are missing, respectively, and we call them ''missing SXRD models'' (models 12–15). Because the result of STM suggested that the coverage of indium should be 0.75,[25] we treated the missing SXRD models carefully. Then we calculated the SXRD model and four missing SXRD models, adding the deeper bulk bilayer. Finally, the R_p of the SXRD model reached 0.151, while the R_p of the missing SXRD models reached 0.182, 0.187, 0.213, and 0.198, respectively. Despite the fact that the R_p values of the missing SXRD models are small, missing SXRD models could be ruled out because those structural parameters were not convergent by several calculations. In addition, $R_p+\Delta R_p$ of the SXRD model is 0.174, which is smaller than the R_p of any of the missing SXRD models. Figure 7 shows the comparison of I-V curves between experimental and theoretical values of the SXRD model. Since the R_p of the SXRD model is sufficiently low and the agreement of I-V curves is good, we conclude that the SXRD model is the appropriate one.

The final atomic positions are listed in Table III. The direction of displacements and the bond lengths derived from the optimized parameters are shown in Fig. 8 and in Table IV, respectively. Compared with the In-In bond length in the element, 3.25 Å, the two In-In distances are remarkably short at 2.91 Å (a-b) and 3.00 Å (c-d), while the other one is 3.24 Å (b-c). The In-Si bond lengths (a-f, d-e, b-1, and c-2) are also shorter (2.51–2.67 Å) than the mean bond length of the In-In and Si-Si bond lengths in the elements, 2.80 Å, while they are similar to the sum of the covalent radii of In and Si, 2.55 Å. In contrast, the Si-Si bonds (e-f and f-4) are extended (2.43 and 2.40 Å, respectively), while the other Si-Si bond (e-3) has almost the same value (2.33 Å) as the Si-Si bond length in the element, 2.35 Å. Though we did not use the Keating method[38] to consider stresses, LEED analysis could obtain reasonable structural parameters for silicon substrate layers. Moreover, the obtained structural parameters are in good agreement with the SXRD and theoretical studies,[24–27] and bond lengths are compared in Table IV. The agreement between the present and SXRD studies are good except for Si-Si bond lengths of e-3 and f-4, where the SXRD results show apparently larger values.

If we neglect the bonds between In(b) and In(c), all indium atoms have three bonds: one with a silicon atom and the other two with indium atoms. And all of the bond lengths

TABLE III. Optimum parameters of the best-fit structure for the Si(111)-(4×1)-In structure (SXRD model). The axes of coordinates are shown in Fig. 8. The surface unit cell is shown in Fig. 8(a) as a dotted rectangle with the size of 13.30 Å×3.84 Å.

	$[\bar{1}\bar{1}2]$ (Å)	$[1\bar{1}0]$ (Å)	[111] (Å)
In (a)	11.50±0.23	1.92	9.26±0.04
In (b)	0.35±0.18	0.00	8.88±0.04
In (c)	2.96±0.21	1.92	8.83±0.05
In (d)	5.22±0.24	0.00	9.26±0.05
Si (e)	7.59±0.10	0.00	8.44±0.02
Si (f)	9.07±0.12	1.92	8.37±0.02
Si (1)	−0.02±0.31	0.00	6.24±0.06
Si (2)	3.31±0.16	1.92	6.19±0.04
Si (3)	6.85±0.26	0.00	6.22±0.05
Si (4)	9.96±0.26	1.92	6.15±0.06
Si (5)	12.20±0.23	1.92	5.49±0.05
Si (6)	2.34±0.20	0.00	5.40±0.05
Si (7)	5.52±0.19	1.92	5.48±0.05
Si (8)	9.19±0.20	0.00	5.19±0.07
Si (9)	12.08±0.22	1.92	3.16±0.04
Si (10)	2.30±0.18	0.00	3.10±0.05
Si (11)	5.50±0.23	1.92	3.15±0.05
Si (12)	8.95±0.14	0.00	2.97±0.04
Si (13)	11.13±0.37	0.00	2.33±0.07
Si (14)	0.87±0.32	1.92	2.38±0.07
Si (15)	4.51±0.29	0.00	2.34±0.07
Si (16)	7.64±0.41	1.92	2.22±0.15

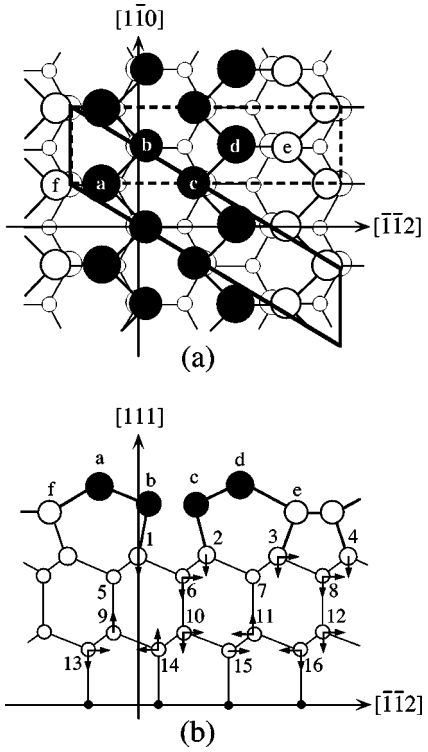

FIG. 8. (a) Top and (b) side views of the best-fit Si(111)-(4×1)-In structure (SXRD model). Solid and open spheres are indium atoms and silicon atoms, respectively. Arrows indicate the directions of displacements from bulk-terminated sites. The parallelogram indicates a (4×1) unit cell, and the dotted rectangle indicates an alternative (4×1) unit cell.

and bond angles suggest reasonable formation of covalent bonds without any dangling bond as mentioned in the theoretical studies.[25,26] However, we emphasize again that the distance of In(b) and In(c) is the same as the In-In bond length in the element, as mentioned in Ref. 27.

C. Phase transition of the (4×1) structure at low temperature

On cooling the (4×1) sample, eighth-order spots and half-order streaks appeared on the (4×1) LEED pattern below 130 K. A LEED pattern at 80 K is shown in Fig. 4(c). In this pattern, the $((2m+1)/8,0)$ spots, where m is any integer, along the (1 0) direction, were missing at all electron energies, as reported in a recent SXRD study.[39] Therefore, we suggest that, as a general rule, the (8×"2") should be called the (8×1)-$p1g1$ with half-order streaks.

In this study we could not obtain certain structural parameters for the low-temperature phase, because the unit cell became large and the symmetry became low, $p1g1$. Therefore, the number of structural parameters became too much to converge. Furthermore, the measurable energy ranges of the eighth-order beams were limited. However, we can empirically conclude that the difference in structural parameters of the (4×1) and (8×1)-$p1g1$ should be very small, because their I-V curves are almost identical, as shown in Fig. 5. In fact, we calculated the (4×1) structure also using I-V curves of the (8×1)-$p1g1$, and similar structural parameters were obtained. In the calculation we used 15 symmetrically inequivalent beams of the (8×1)-$p1g1$ without eighth-order beams, and the total-energy range E_t was 2493 eV. Thus obtained structural parameters were similar to those in Table III. In contrast, the structural parameters obtained by SXRD analysis at low temperature show rather large differences from those obtained at RT.[24,39]

With regard to diffraction patterns, there are four characteristic elements related to the structure of the low-temperature phase: (1) eighth-order spots, (2) glide plane symmetry, (3) streaks appearing at the half-order position, and (4) the same streaks expanding along the (1 0) direction. Eighth-order spots and glide plane symmetry are both related to the (8×1)-$p1g1$ structure, having long-range order. On the other hand, half-order streaks indicate the presence of short-range order, and the element (3) should be considered separately from the element (4). The presence or absence of dependence between eighth-order spots and half-order streaks is an interesting aspect. In other words, clarification of the relationship between the (8×1)-$p1g1$ structure and twofold periodicity modulation of the STM images is of interest. In our experiments, the half-order streaks appeared simultaneous with the eighth-order spots, and the width of the streaks was always narrow. Therefore, it is plausible to say that the twofold periodicity modulations in the indium chains have long-range order along indium chains when the (8×1)-$p1g1$ structure has been achieved. This means that elements (1), (2), and (3) have the same origin and appear at

TABLE IV. List of bond lengths for the Si(111)-(4×1)-In structure.

Bond	LEED (Å) (present)	SXRD (Å) (Ref. 24)	Bond length in the element (Å)
In (a) – In (b)	2.91	2.99	3.25
In (b) – In (c)	3.24	3.15	3.25
In (c) – In (d)	3.00	2.97	3.25
In (a) – Si (f)	2.59	2.62	2.80 [a]
In (d) – Si (e)	2.51	2.50	2.80
In (b) – Si (1)	2.66	2.56	2.80
In (c) – Si (2)	2.67	2.74	2.80
Si (e) – Si (f)	2.43	2.40	2.35
Si (e) – Si (3)	2.33	2.54	2.35
Si (f) – Si (4)	2.40	2.55	2.35

[a]An average value of the In-In and Si-Si bond lengths in the elements.

the same time. If the twofold periodicity modulation has pure one-dimensional property, the simultaneous appearing of the eighth-order spots is not inevitable. Our LEED analysis suggests that the atomic displacements due to the twofold periodicity modulation might be small. Since STM images are sensitive to the valence electrons, the small displacements would produce bright cocoons.[16,36] The cocoons have well-ordered twofold periodicity in the indium chains, corresponding to the element (3) of the LEED pattern. Another feature of the cocoons is their tilting directions. There are two opposite directions of the tilt angle. The neighboring rows have alternate tilt angles, making well-developed eighthfold periodicity perpendicular to the indium chains [the element (1) of the LEED pattern]. On the other hand, the relative position of the cocoons along the [112] direction is not definite,[36] since there are two equivalent arrangements, which is suggested by Kumpf *et al.* [Figs. 4(a) and 4(b) of Ref. 39]. As a result, the streaks appear along the (1 0) direction, and the streaks will not converge to spots even at low temperatures.[39] Therefore, we have to separate the element (4) from the other three elements.

Consequently one can make a following scenario of the phase transition. At first, the pairing of the indium chains occur. Then, silicon atoms in zigzag chains are drawn by the indium atoms. Since the displacements of the silicon zigzag chains occur in opposite directions in neighboring rows, these effects spread in the $[\overline{112}]$ direction alternatively, and the silicon atoms form the (8×1)-$p1g1$ structure. This description fits that of a typical charge density wave formation. In this case, the streaks also appear along the (1 0) direction, and the streaks will not converge to spots at low temperatures when the (8×1)-$p1g1$ structure of silicon atoms has been completed. Thus, the remaining streakiness does not support the premise that the phase transition is not driven by a charge density wave. On the other hand, we cannot deny another possible scenario for the phase transition caused by a different origin. At first, Si atoms form the (8×1)-$p1g1$ structure, although the reason for it is unknown. The formation of the (8×1)-$p1g1$ structure modulates the bonding nature of indium atoms, and a doubling of the indium chains takes place. It is not possible to distinguish these two scenarios at this stage. Further theoretical studies are necessary to deepen the current understanding, but we would like to emphasize that the low-temperature phase should be treated as (8×1)-$p1g1$ with twofold modulations structure, but should not be treated as a (4×2) structure. The eighthfold periodicity along the [112] direction should be as important as the twofold periodicity along the [110] direction.

IV. SUMMARY

We determined the atomic structures of the $(\sqrt{3}\times\sqrt{3})R30°$ and the (4×1) structures quantitatively. The T_4 model is the best-fit model of the $(\sqrt{3}\times\sqrt{3})$ structure, and indium adatoms maintain the characteristics of the group-13 elements. For the (4×1) structure, we analyzed 45 models, consisting of three basic models proposed by SXRD, TED, and STM studies, and modified models. The results suggested that the SXRD model was appropriate. The low-temperature phase, the (8×1)-$p1g1$ with half-order streaks, has I-V curves similar to those of the (4×1) phase. Our results suggest that the phase transition is accompanied by slight displacements to produce glide plane symmetry and twofold periodicity modulation in indium rows.

ACKNOWLEDGMENTS

This work was supported in part by a Grand-in-Aid for Scientific Research (No. 13440097) and a Japan-Korea collaboration program supported by JSPS and KOSEF. One of the authors (Y.O.M.) acknowledges the support of the JSPS for Young Scientists.

[1] V. G. Lifshits, A. A. Saranin, and A. V. Zotov, *Surface Phases on Silicon* (Wiley, New York, 1994).
[2] J. J. Lander and J. Morrison, Surf. Sci. **2**, 553 (1964).
[3] J. Nogami, S.-I. Park, and C. F. Quate, J. Vac. Sci. Technol. B **6**, 1479 (1988).
[4] K. Izumi, T. Takahashi, and S. Kikuta, Jpn. J. Appl. Phys., Part 1 **28**, 1742 (1989).
[5] N. Nakamura, K. Anno, and S. Kono, Surf. Sci. **262**, L101 (1992).
[6] D. M. Cornelison, C. S. Chang, and I. S. T. Tsong, J. Vac. Sci. Technol. A **8**, 3443 (1990).
[7] J. M. Nicholls, P. Mårtensson, G. V. Hansson, and J. E. Northrup, Phys. Rev. B **32**, 1333 (1985).
[8] J. M. Nicholls, B. Reihl, and J. E. Northrup, Phys. Rev. B **35**, 4137 (1987).
[9] M. S. Finney, C. Norris, P. B. Howes, R. G. van Silfhout, G. F. Clark, and J. M. C. Thornton, Surf. Sci. **291**, 99 (1993).
[10] T. Hanada, H. Daimon, and S. Ino, Phys. Rev. B **51**, 13 320 (1995).
[11] J. Nogami, S.-I. Park, and C. F. Quate, Phys. Rev. B **36**, 6221 (1987).
[12] J. Kraft, M. G. Ramsey, and F. P. Netzer, Phys. Rev. B **55**, 5384

(1997).
[13] T. Abukawa, M. Sasaki, F. Hisamatsu, T. Goto, T. Kinoshita, A. Kakizaki, and S. Kono, Surf. Sci. **325**, 33 (1995).
[14] I. G. Hill and A. B. McLean, Phys. Rev. B **56**, 15 725 (1997).
[15] I. G. Hill and A. B. McLean, Phys. Rev. B **59**, 9791 (1999).
[16] H. W. Yeom, S. Takeda, E. Rotenberg, I. Matsuda, K. Horikoshi, J. Schaefer, C. M. Lee, S. D. Kevan, T. Ohta, T. Nagao, and S. Hasegawa, Phys. Rev. Lett. **82**, 4898 (1999).
[17] H. W. Yeom, K. Horikoshi, H. M. Zhang, K. Ono, and R. I. G. Uhrberg, Phys. Rev. B **65**, 241307 (2002).
[18] D. M. Cornelison, M. S. Worthington, and I. S. T. Tsong, Phys. Rev. B **43**, 4051 (1991).
[19] J. L. Stevens, M. S. Worthington, and I. S. T. Tsong, Phys. Rev. B **47**, 1453 (1993).
[20] N. Nakamura, K. Anno, and S. Kono, Surf. Sci. **256**, 129 (1991).
[21] A. A. Saranin, A. V. Zotov, K. V. Ignativoch, V. G. Lifshits, T. Numata, O. Kubo, H. Tani, M. Katayama, and K. Oura, Phys. Rev. B **56**, 1017 (1997).
[22] C. Collazo-Davilla, L. D. Marks, K. Nishi, and Y. Tanishiro, Surf. Rev. Lett. **4**, 65 (1997).
[23] M. S. Finney, C. Norris, P. B. Howes, M. A. James, J. E. Macdonald, A. D. Johnson, and E. Vlieg, Physica B **198**, 246 (1994).
[24] O. Bunk, G. Falkenberg, J. H. Zeysing, L. Lottermoser, R. L. Johnson, M. Nielsen, F. Berg-Rasmussen, J. Baker, and R. Feidenhans'l, Phys. Rev. B **59**, 12 228 (1999).
[25] R. H. Miwa and G. P. Srivastava, Surf. Sci. **473**, 123 (2001).
[26] J. Nakamura, S. Watanabe, and M. Aono, Phys. Rev. B **63**, 193307 (2001).
[27] J.-H. Cho, D.-H. Oh, K. S. Kim, and L. Kleinman, Phys. Rev. B **64**, 235302 (2001).
[28] A. A. Saranin, A. V. Zotov, V. G. Lifshits, J.-T. Ryu, O. Kubo, H. Tani, T. Harada, M. Katayama, and K. Oura, Phys. Rev. B **60**, 14 372 (1999); A. V. Zotov, A. A. Saranin, O. Kubo, T. Harada, M. Katayama, and K. Oura, Appl. Surf. Sci. **159**, 237 (2000).
[29] M. A. Van Hove, W. Moritz, H. Over, P. J. Rous, A. Wander, A. Barbieri, N. Materer, U. Starke, and G. A. Somorjai, Surf. Sci. Rep. **19**, 191 (1993).
[30] H. Huang, S. Y. Tong, J. Quinn, and F. Jona, Phys. Rev. B **41**, 3276 (1990).
[31] N. Sato, T. Nagao, and S. Hasegawa, Surf. Sci. **442**, 65 (1999).
[32] H. Huang, S. Y. Tong, W. S. Yang, H. D. Shih, and F. Jona, Phys. Rev. B **42**, 7483 (1990).
[33] A. Kawazu and H. Sakama, Phys. Rev. B **37**, 2704 (1988).
[34] J. B. Pendry, J. Phys. C **13**, 937 (1980).
[35] R. E. Martinez, E. Fontes, J. A. Golovchenko, and J. R. Patel, Phys. Rev. Lett. **69**, 1061 (1992).
[36] S. V. Ryjkov, T. Nagao, V. G. Lifshits, and S. Hasegawa, Surf. Sci. **488**, 15 (2001).
[37] T. Abukawa, M. Sasaki, F. Hisamatsu, M. Nakamura, T. Kinoshita, A. Kakizaki, T. Goto, and S. Kono, J. Electron Spectrosc. Relat. Phenom. **80**, 233 (1996).
[38] P. N. Keating, Phys. Rev. **145**, 637 (1966).
[39] C. Kumpf, O. Bunk, J. H. Zeysing, Y. Su, M. Nielsen, R. L. Johnson, R. Feidenhans'l, and K. Bechgaard, Phys. Rev. Lett. **85**, 4916 (2000).